



Numerical investigation of an all-optical logic OR gate at 80 Gb/s with a dual pump–probe semiconductor optical amplifier (SOA)-assisted Mach–Zehnder interferometer (MZI)

Amer Kotb^{1,2} · Kyriakos E. Zoiros³ · Chunlei Guo^{1,4}

© Springer Science+Business Media, LLC, part of Springer Nature 2018

Abstract

The performance of an all-optical OR gate using a dual pump–probe semiconductor optical amplifier (SOA)-assisted Mach–Zehnder interferometer (MZI) is investigated and demonstrated through numerical simulations at a data rate of 80 Gb/s. The proposed scheme enables to obtain a higher quality factor and smaller pattern dependence for a more feasible choice of critical operating parameters than when using for the same purpose the SOA–delayed interferometer.

Keywords All-optical OR gate · Semiconductor optical amplifier · Mach–Zehnder interferometer · Dual pump–probe scheme

1 Introduction

Boolean OR is one of the basic logic operations in the suite of fundamental binary functions [1]. In particular, its execution exclusively by means of light is desirable for enabling all-optical (AO) signal processing tasks in both fundamental and system-oriented level [2]. In line with the progress on AO logic circuits and subsystems achieved owing to semiconductor optical amplifier's (SOA) attractive properties, the implementation of the specific gate and the investigation of its performance have largely been addressed based on this technology [3–6]. To this aim, SOAs have been exploited either with a delayed interferometer (SOA-DI) [7–10] or in the conventionally driven Mach–Zehnder interferometer

(SOA-MZI) [11–14]. In this paper, we propose to employ the SOA-MZI, but in a dual pump–probe configuration, where pairs of the data signals, between which the target Boolean OR operation is executed, are distinctly launched into the MZI acting as pump and probe inside the SOAs. The performance of the all-optical OR gate realized in this way is investigated through numerical simulations run at 80 Gb/s. Compared to the SOA-DI configuration employed to obtain Boolean OR operation at 80 Gb/s [8, 9], the scheme we propose exhibits smaller pattern dependence in a more affordable manner and less stringent operating requirements. Moreover, the results obtained by examining and assessing the influence of the input signals and SOA critical parameters, including the effect of amplified spontaneous emission (ASE), on the quality factor (QF) demonstrate that the latter is well over the critical limit and higher with the conceived, than with the conventional, SOA-based AO circuitry.

2 Theoretical formulation

Electrons and holes will be placed in the conduction and valence bands of each SOA due to the pumping of the injection current. The incoming incident photons are launched into the SOAs active region and collide with electrons in the conduction band to release stimulated photons with the same phase, frequency, and direction. For high intensities, carrier heating (CH) manifests inside each SOA when the temperature of carriers is higher than the lattice temperature. This

✉ Amer Kotb
amer@ciomp.ac.cn

✉ Chunlei Guo
guo@optics.rochester.edu

¹ The Guo China-US Photonics Laboratory, Changchun Institute of Optics, Fine Mechanics, and Physics, Chinese Academy of Sciences, Changchun 130033, China

² Department of Physics, Faculty of Science, University of Fayoum, Fayoum 63514, Egypt

³ Lightwave Communications Research Group, Department of Electrical and Computer Engineering, School of Engineering, Democritus University of Thrace, 67100 Xanthi, Greece

⁴ The Institute of Optics, University of Rochester, Rochester, NY 14627, USA

process occurs on a time scale of 0.7–1 ps. Also, a high optical intensity burns a hole in the gain spectrum, which is known as spectral hole burning (SHB). These nonlinear processes are very fast and should not be neglected when pursuing to provide an accurate theoretical description of SOAs behavior. The operation of the SOA-MZI can be theoretically studied as detailed in [15–20]. The SOA-MZI time-dependent gains due to interband carrier depletion (CD) and CH, SHB effects are derived from the solution of the following first-order differential equations, respectively [2, 21]:

$$\frac{dh_{CD}(t)}{dt} = \frac{h_0 - h_{CD}(t)}{\tau_C} - (\exp[h_{CD}(t) + h_{CH}(t) + h_{SHB}(t)] - 1) \frac{P(t)}{E_{sat}} \quad (1)$$

$$\frac{dh_{CH}(t)}{dt} = -\frac{h_{CH}(t)}{\tau_{CH}} - \frac{\varepsilon_{CH}}{\tau_{CH}} (\exp[h_{CD}(t) + h_{CH}(t) + h_{SHB}(t)] - 1) P(t) \quad (2)$$

$$\frac{dh_{SHB}(t)}{dt} = -\frac{h_{SHB}(t)}{\tau_{SHB}} - \frac{\varepsilon_{SHB}}{\tau_{SHB}} (\exp[h_{CD}(t) + h_{CH}(t) + h_{SHB}(t)] - 1) P(t) - \frac{dh_{CD}(t)}{dt} - \frac{dh_{CH}(t)}{dt}, \quad (3)$$

where functions ‘ h ’ represent the SOAs gain integrated over their length due to CD, CH, and SHB (hence the corresponding subscripts). $h_0 = \ln[G_0]$, where G_0 is the SOAs unsaturated gain. $E_{sat} = P_{sat} \tau_c$ is the SOAs saturation energy, where P_{sat} is the SOAs saturation power and τ_c is the SOAs carrier lifetime. $P(t)$ is the input signal power. τ_{CH} and τ_{SHB} are the temperature relaxation rate and the carrier–carrier scattering rate, respectively. ε_{CH} and ε_{SHB} are the nonlinear gain suppression factors due to CH and SHB, respectively.

The total gain $G(t)$ in each SOA-MZI arm is given by [2, 21]:

$$G(t) = \exp[(h_{CD}(t) + h_{CH}(t) + h_{SHB}(t))]. \quad (4)$$

The phase change is linked to the total gain through the involved linewidth enhancement factors. The value of α_{SHB} is null because SHB produces a nearly symmetrical spectral hole centered at the signal wavelength and the Kramers–Kronig integral remains very small [22–24]. The phase change of the input signal propagating through the SOAs is given by [2, 21]:

$$\Phi(t) = -0.5(\alpha h_{CD}(t) + \alpha_{CH} h_{CH}(t) + \alpha_{SHB} h_{SHB}(t)), \quad (5)$$

where α is the traditional linewidth enhancement factor (α -factor). α_{CH} and α_{SHB} are the linewidth enhancement factors due to CH and SHB, respectively.

In the simulation, the input data streams A and B are assumed to be Gaussian-shaped with power profile described by [22–24]:

$$P_{A,B}(t) \equiv P(t) = \sum_{n=1}^N a_{nA,B} \frac{2\sqrt{\ln(2)}E_0}{\sqrt{\pi}\tau_{FWHM}} \exp\left[-\frac{4\ln(2)(t-nT)^2}{\tau_{FWHM}^2}\right], \quad (6)$$

where $\alpha_{nA,B}$ is ‘1’ or ‘0’ inside a $N = 2^7 - 1$ bit-long pseudo-random binary sequence (PRBS) of pulses having energy E_0 , full width at half maximum (FWHM) pulse width τ_{FWHM} , and period T . The total power that enters SOA1 and SOA2 in the two MZI arms is, respectively:

$$P_1(t) = P_{A_{pump}}(t) + P_{B_{pump}}(t) + 0.5(P_{A_{probe}}(t) + P_{B_{probe}}(t)) \quad (7)$$

$$P_2(t) = 0.5(P_{A_{probe}}(t) + P_{B_{probe}}(t)). \quad (8)$$

The schematic diagram and truth table of the all-optical OR gate based on the dual pump–probe SOA-MZI are shown in Fig. 1.

In order to implement the OR operation between two data streams A and B , the latter are inserted in the upper MZI arm acting as ‘pump signals,’ as denoted by ‘Data A_{pump} ’ and ‘Data B_{pump} ,’ respectively. Concurrently, signals of same binary content but much lower intensity enter the upper and lower MZI arms having the role of the ‘probe,’ as denoted by ‘ A_{probe} ’ and ‘ B_{probe} ,’ respectively, on which the nonlinear effects induced inside the SOAs by the pump signals are mapped and transformed into switching. Using in this dual way the signals between which the target logic operation is going to be executed, i.e., identical signals are inserted from different inputs having different roles, is a practice that has been exploited before for implementing all-optical Boolean functions [25]. It should be noted that although the combination of signals A and B can be viewed as an effective OR operation, this is realized passively by means of wavelength-selective couplers (WSCs), which cannot substitute the active function of the MZI. Thus, WSCs provide just the composite of different wavelengths, at which signals A and B are spectrally located so that they can be discriminated from each other, for further exploitation in a nonlinear active device (in this case the SOA). In contrast, the MZI acts on optical time-division-multiplexed data streams and produces a logical outcome at a bit-slotted level on a single wavelength. Therefore, the WSCs have only a supporting role and provided they are chosen to exhibit low insertion losses and wide bandwidth in the optical communications C-band spectral

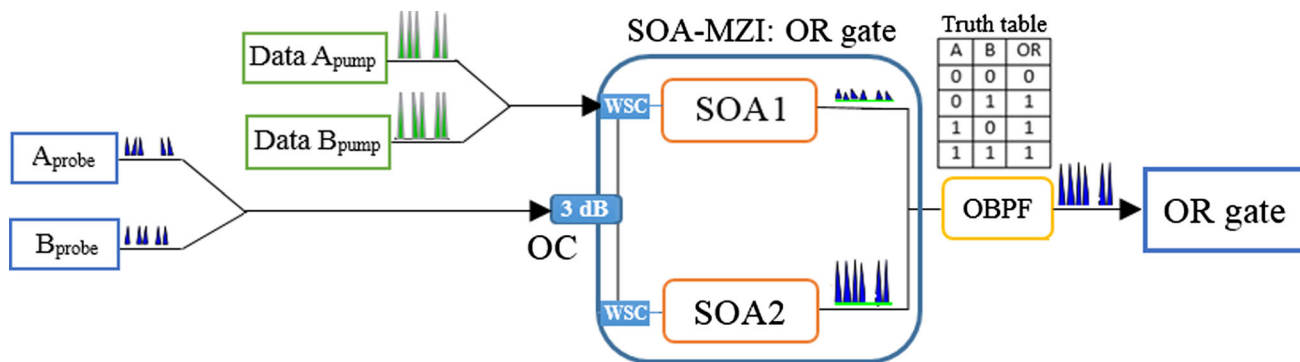


Fig. 1 Schematic diagram and truth table of the dual pump–probe SOA-MZI OR gate, OC 3 dB optical coupler, WSC wavelength-selective coupler, and OBPF optical bandpass filter

region, which is practically feasible with the commercially available versions of these elements, they are not capable of affecting the overall performance of the AO logic system. The operation of this circuit relies on cross-gain modulation (XGM) inside each SOA by the stronger pump signals on their weaker probe counterparts, to which their binary content must be adjusted to coincide, and subsequently on cross-phase modulation (XPM) incurred by the associated changes of the SOAs gain dynamics. More specifically, when the binary content of A and B pump and probe combination $(A + B)_{\text{pump}}$ and $(A + B)_{\text{probe}}$, respectively, is ‘0’, which happens when $A_{\text{pump, probe}} = ‘0’$ and $B_{\text{pump, probe}} = ‘0’$, the two SOAs remain in steady state and accordingly the two MZI arms are balanced, so that no XPM manifests and there is no output, i.e., a logical ‘0’. In contrast, when both $(A + B)_{\text{pump}}$ and $(A + B)_{\text{probe}}$ are ‘1’, which happens when either $A_{\text{pump, probe}}$, $B_{\text{pump, probe}}$, or both of them, are ‘1’, then subject to XGM in SOA1 the respective traveling probe signals perceive a dynamically suppressed gain, while in the absence of pump input in SOA2 they experience an unsaturated gain. This process creates a gain difference, which, through XPM, is translated into constructive interference at the MZI output and into a logical ‘1’. In this manner, the OR operation is executed between A and B according to the truth table of this Boolean function. The output power of the OR gate is given by the following interferometric equation [21]:

$$P_{\text{OR}}(t) = 0.25(P_{A_{\text{probe}}}(t) + P_{B_{\text{probe}}}(t))(G_1(t) + G_2(t) - 2\sqrt{G_1(t)G_2(t)}\cos[\Phi_1(t) - \Phi_2(t)]), \quad (9)$$

where $G_{1,2}(t)$ and $\Phi_{1,2}(t)$ are the time-dependent total gains and phase shifts incurred inside MZI SOA1 and SOA2, respectively. The performance of the OR gate depends on the input signals and SOAs parameters, which should be properly selected for optimum performance. The default values of the SOAs physical and structural parameters as well as of the optical pulses parameters used in the conducted simulation are given in Table 1 [2, 11, 26].

Table 1 Simulation parameters

Parameter	Symbol	Value	Unit
Length of active region	L	0.5	mm
Thickness of active region	d	0.1	μm
Width of active region	w	2	μm
Injection current	I	250	mA
Carrier lifetime	τ_c	200	ps
Traditional linewidth enhancement factor	α	5	–
Linewidth enhancement factor due to CH	α_{CH}	1	–
Linewidth enhancement factor due to SHB	α_{SHB}	0	–
Temperature relaxation rate	τ_{CH}	0.3	ps
Carrier–carrier scattering rate	τ_{SHB}	0.1	ps
Nonlinear gain suppression factor due to CH	ε_{CH}	0.2	W^{-1}
Nonlinear gain suppression factor due to SHB	ε_{SHB}	0.2	W^{-1}
Unsaturated power gain	G_0	30	dB
Saturation power	P_{sat}	30	mW
Pulse energy	E_0	0.1	pJ
Pulse width	τ_{FWHM}	0.5	ps
Bit period	T	12.5	ps
Optical bandwidth	B_0	3	nm
Spontaneous emission factor	N_{sp}	2	–

3 Results and discussion

The performance of the all-optical OR gate based on the dual pump–probe SOA-MZI has been investigated and evaluated by means of the QF. This metric is defined as [23] $\text{QF} = (P_1 - P_0)/(\sigma_1 + \sigma_0)$, where $P_{0,1}$ are the average powers of the logical ‘0’s and ‘1’s and $\sigma_{0,1}$ are the corresponding standard deviations. Figure 2 shows the input data A , B , as well as the logical result and corresponding eye diagram of the OR gate.

Fig. 2 Simulation results for dual pump–probe SOA-MZI OR gate: **a** input data A, **b** input data B, **c** OR output, **d** corresponding eye diagram. The QF is found to be 11 at a data rate of 80 Gb/s

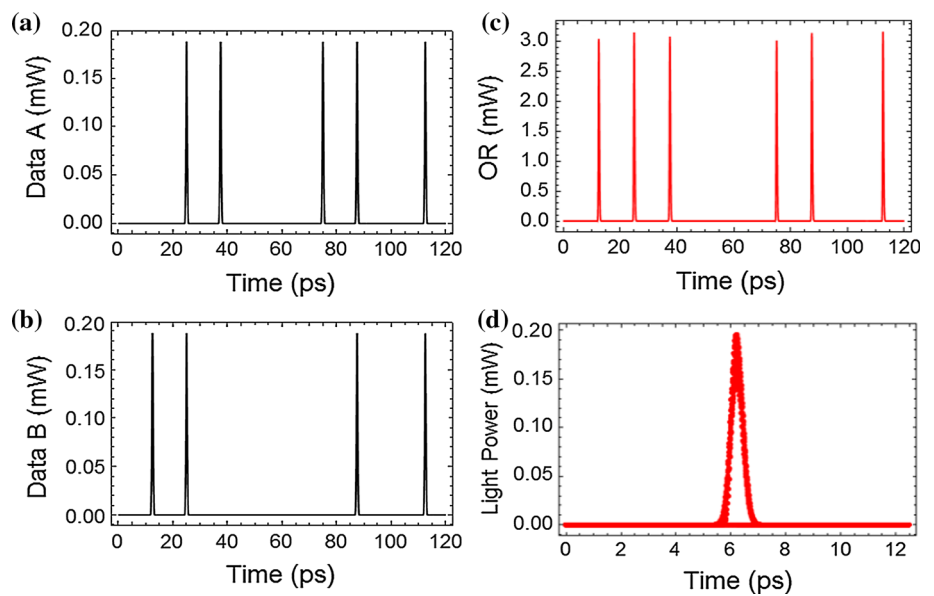
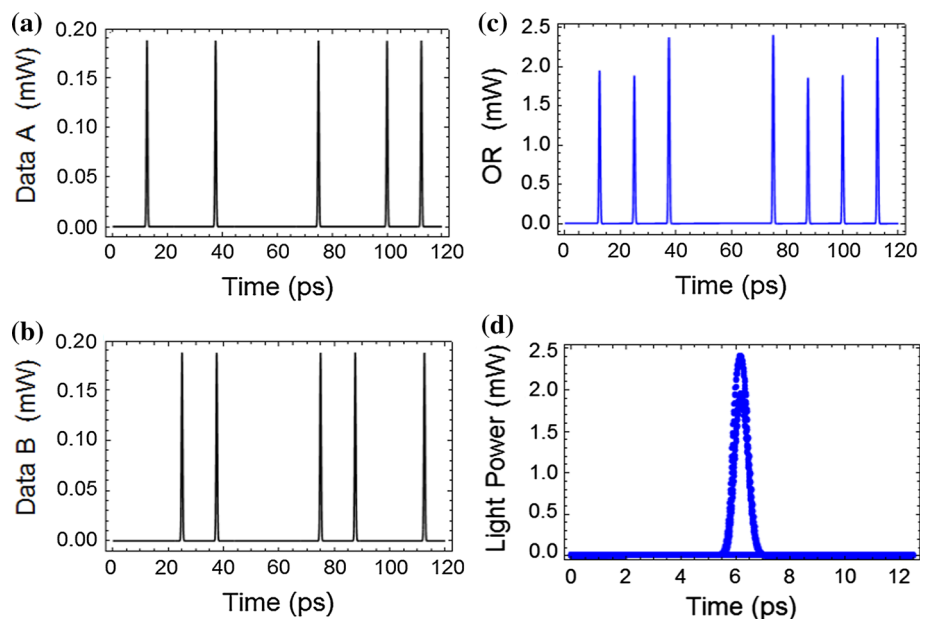


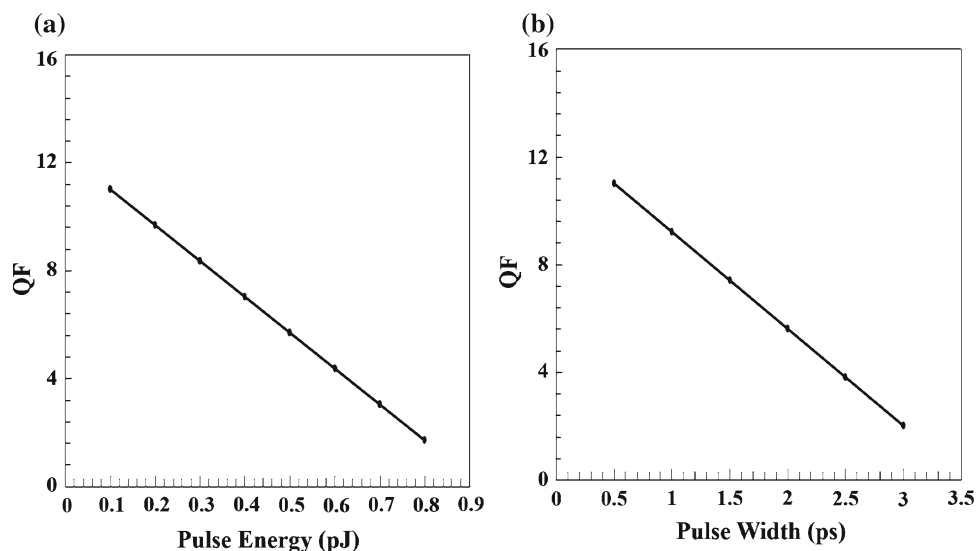
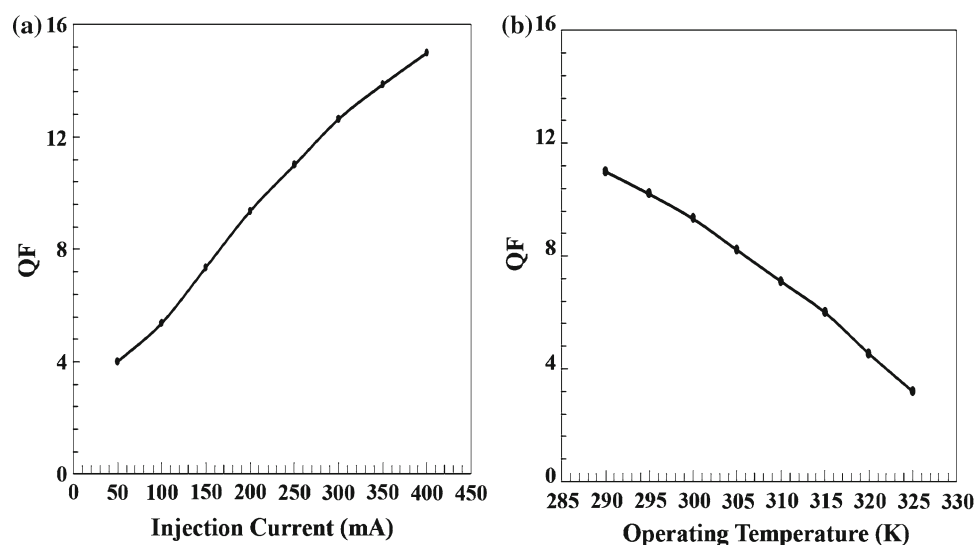
Fig. 3 Simulation results for SOA-DI OR gate: **a** input data A, **b** input data B, **c** OR output, **d** corresponding eye diagram. The QF is found to be 7.4 at 80 Gb/s



In particular, when $A = B = '1'$, it is shown in Fig. 2c that despite the higher pump intensity that in this case increases the induced XPM, still the quality of the OR outcome is not impaired. This happens because although the MZI level of interference is analogously affected, this happens to an extent that the concomitant differential phase, i.e., the argument of the cosine term in interferometric Eq. (9), is made to lie in the vicinity of an odd multiple of π , which is desirable for achieving almost full switching. These results confirm that driving the SOA-MZI according to the proposed configuration allows executing the OR gate with both logical correctness and high quality. The calculated QF is 11 at a data rate of 80 Gb/s, which is higher than when using the SOA-DI, for which the QF is 7.4. The small peak amplitude

variations in the output logic '1's are caused by pattern effects due to the relatively long SOAs carrier lifetime, which results in slower gain-induced phase changes, as well as due to the ASE effect. Compared to Fig. 3, which depicts the same set of simulation results obtained for the SOA-DI by calculating its response [8, 9] for DI delay and phase bias values of 0.1 ps and π rad, respectively, the proposed dual pump–probe scheme notably exhibits smaller pattern dependence than the SOA-DI, which is a fact that together with the increased QF highlights its better performance potential.

The QF depends on the input pulses energy and width, as shown in Fig. 4a and b, respectively. A higher input signal energy causes a heavier SOAs gain saturation, which impairs the process of switching, and the QF is dropped, as shown

Fig. 4 QF versus input pulses **a** energy and **b** width**Fig. 5** QF versus SOAs **a** injection current and **b** operating temperature

in Fig. 4a. Thus, a comparatively lower pulse energy is sufficient, which can be provided more easily from available optical pulse generation systems. A similar trend is observed in Fig. 4b concerning the dependence of the QF on the input pulse width. The QF is decreased as input pulses become broader, which causes stronger SOAs saturation. The pulses tend to overlap for a wider pulse width, which causes higher pattern effects on the OR output. These figures indicate that input pulse energies as low as 0.1 pJ and narrow input pulses in the sub-picosecond regime can support acceptable OR gate performance.

Carriers are supplied to the SOAs active region through the bias current. As shown in Fig. 5a, the QF inclines by injecting more current, which, however, results in increased electrical power consumption. On the other hand, a more than acceptable QF can be obtained for lower values of this parameter. Thus, a compromise between these two extremes

can efficiently be made by selecting a medium bias current value of the order of 250 mA. Figure 5b shows the QF dependence on the SOAs operating temperature. The QF is higher at lower temperatures. Physically, this happens because the distribution of free carriers and the non-radiative recombination become such that they favor the supply of more gain [27], which in turn causes the QF to increase. First, the probability of carriers to occupy the active medium energy levels is increased with temperature drop. Second, electrons are distributed over a narrow range at a lower temperature and hence the number of these carriers available for participating in optical transitions to provide amplification is enhanced. Third, non-radioactive recombinations, which decrease with temperature declination, cause the gain to increase for a given current. Moreover, the temperature decrease accelerates the SOAs gain recovery [27], which hence becomes more capable of handling ultrafast data and hence supporting OR

Fig. 6 QF versus SOAs active region **a** length and **b** thickness

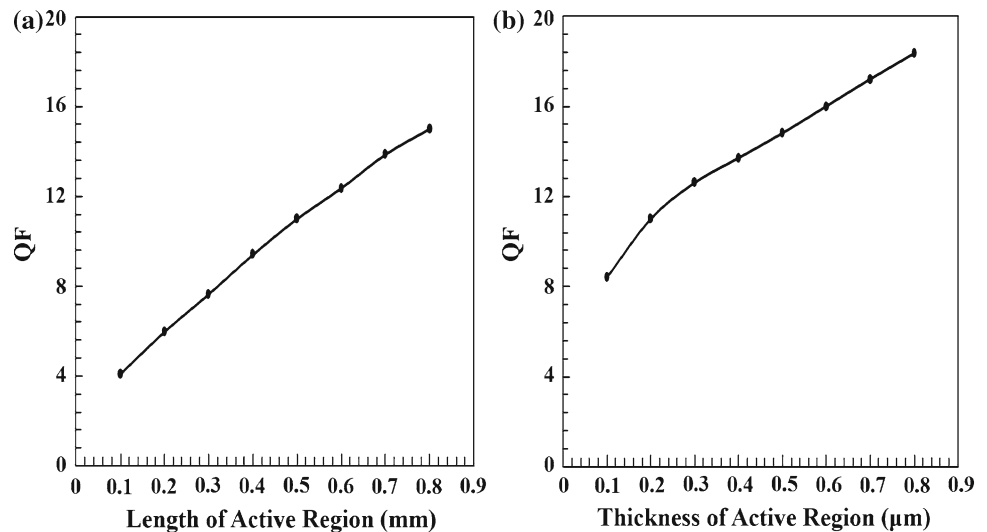
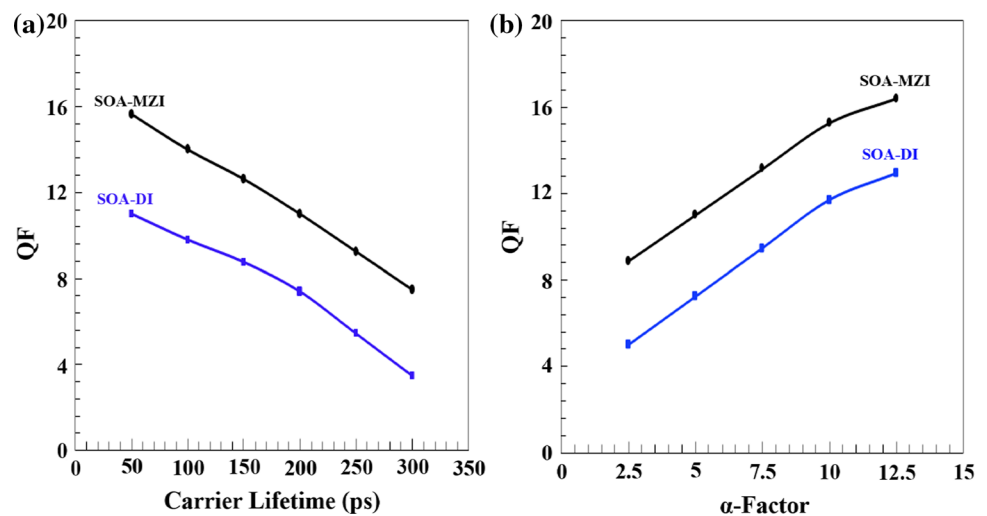


Fig. 7 QF versus SOAs **a** carrier lifetime and **b** α -factor for SOA-MZI and SOA-DI OR gate



operation with improved performance. Therefore, the SOAs operating temperature should be kept low, which is feasible with the temperature control circuitry that accompanies for this purpose real SOA devices.

The QF versus the length and thickness of the SOAs active region is shown in Fig. 6a and b, respectively. From Fig. 6a it is noticed that the QF is increased in a longer SOA active region, as in this case more gain is available for nonlinear switching. A qualitatively similar observation can be made from Fig. 6b with regard to the thickness of the SOAs active region. Therefore, higher QFs can be obtained when using larger, i.e., less compact, SOA devices. This in turn means that where system requirements dictate keeping device footprint small, higher injection currents will, according to Fig. 5a, be required to obtain still high values of this performance metric, at the expense of increased power consumption.

Figure 7a and b shows the dependence of the QF on the SOAs carrier lifetime and traditional linewidth enhancement

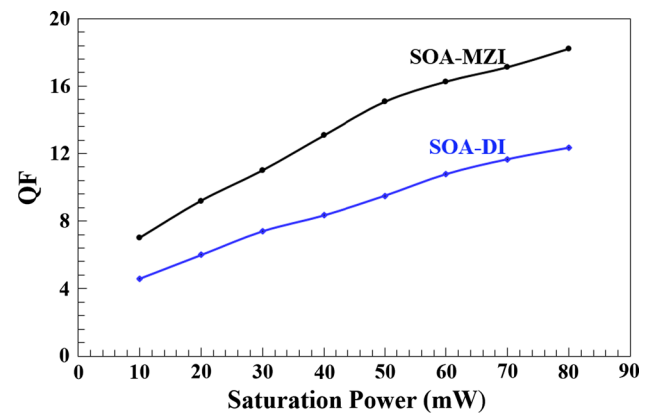


Fig. 8 QF versus SOAs saturation power for SOA-MZI and SOA-DI OR gate

factor (α -factor), for the SOA-assisted MZI- and DI-based OR operations. The carrier lifetime is a very important parameter in the amplification process. A longer lifetime

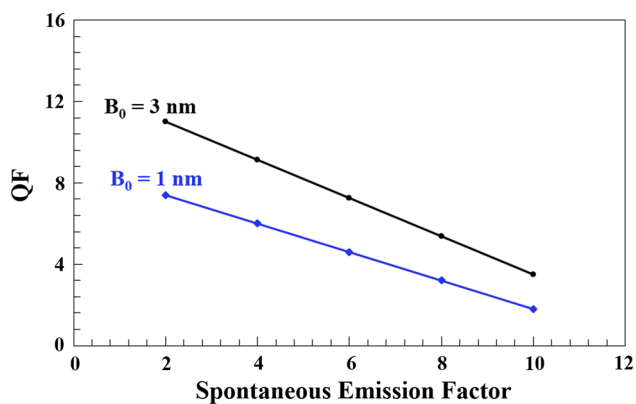


Fig. 9 QF versus SOAs spontaneous emission factor for different optical bandwidths

results in slower carrier replenishment at the given data rate, which decreases the QF, as shown in Fig. 7a. Nevertheless, the QF can be kept acceptable for the SOA-MZI even if the SOAs carrier lifetime is quite longer with respect to the repetition period, while for the SOA-DI the allowable ratio τ_c/T must be more confined. This fact is a physical by-product of the dual pump–probe scheme which accelerates the SOAs response to ultrafast data, at the expense of using extra laser sources for making available the necessary input signals [11]. On the other hand, the QF is increased for higher α -factor values, as shown in Fig. 7b. For a smaller α -factor, the QF using SOA-MZI is acceptable and higher than with SOA-DI. This difference, which relaxes the operating requirements with regard to the selection of the specific parameter [28], can be attributed to the dual pump–probe configuration, which induces a stronger phase shift and hence level of switching.

The QF depends on the SOAs saturation power, as shown in Fig. 8 for the SOA-MZI- and SOA-DI-based OR operation. It is seen that although the QF is increased in both cases, it becomes acceptable only when using the SOA-MZI. For a

realistic saturation power of 30 mW, i.e., ~ 15 dBm, the QF is 11 when using the SOA-MZI and 7.4 when using the SOA-DI.

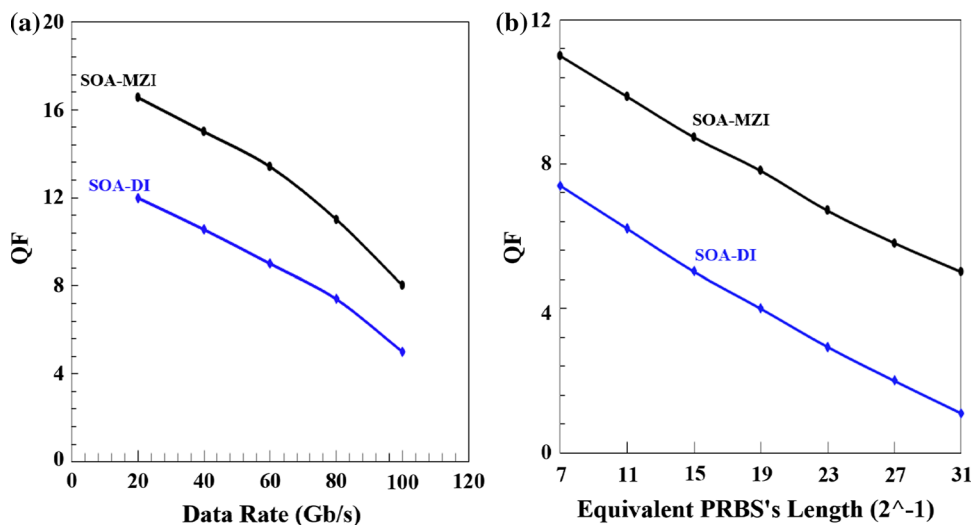
The simulation of the SOA accounts for the effect of the amplified spontaneous emission (ASE), which plays a significant role in the performance of the logic gate. The ASE occurs during the amplification process due to the spontaneous emission and is considered as a source of noise that causes pulse distortion, which degrades the QF. Thus, in this simulation, we include the contribution of this effect, which is numerically added to the OR output power by the following equation [29]:

$$P_{ASE} = N_{sp}(2\pi\hbar(G_0 - 1))\nu B_0, \tag{10}$$

where N_{sp} is the SOA spontaneous emission factor, \hbar is normalized Planck’s constant, B_0 is the optical bandwidth, and ν is the optical frequency. The QF versus N_{sp} is shown in Fig. 9 for $B_0 = 1 \text{ nm}$, 3 nm , $G_0 = 30 \text{ dB}$, and $\nu = 200 \text{ THz}$. The performance of the OR gate remains acceptable even in the presence of ASE. Also, narrower optical bandwidths reject more strongly the noise and hence are favorable for the performance of the OR gate, which is feasible with commercially available optical filters.

The variation of the QF with the data rate and equivalent PRBS length for the SOA-MZI and SOA-DI is shown in Fig. 10a and b, respectively. The QF drops when the operating data rate is increased, as observed in Fig. 10a, but it remains over the limit of 6 for the SOA-MZI case even up to 100 Gb/s, while this is not possible with the SOA-DI. On the other hand, Fig. 10b shows how sensitive the performance of the OR gate is to the equivalent PRBS length [30]. This represents the number of consecutive ‘0’s and ‘1’s contained in each data sequence driving the SOAs in the MZI according to the PRBS ‘balance’ property, which states that if the PRBS order is ‘ r ’ then it contains ‘ $r - 1$ ’ consecutive zeros and

Fig. 10 QF versus **a** data rate and **b** equivalent PRBS length for SOA-MZI and SOA-DI OR gate



' r ' consecutive ones. This numerical approach is more computationally affordable than if the full PRBS length, which scales with the power of '2', i.e., $2^r - 1$, were used instead. The equivalent PRBS length that corresponds to these strings can sufficiently stress the performance of the OR gate which, as shown in Fig. 10b, can support operation for higher number of bits when realized with the SOA-MZI than with the SOA-DI.

4 Conclusion

In conclusion, the performance of an all-optical OR gate using a dual pump–probe semiconductor optical amplifier (SOA)-assisted Mach–Zehnder interferometer (MZI) configuration was numerically simulated, investigated, and analyzed at 80 Gb/s. The obtained results show that, provided that the parameters of the input signals and SOAs are suitably chosen, the OR gate implemented with the proposed SOA-MZI scheme exhibits better performance and higher quality factor than when using a SOA–delayed interferometer.

References

- Mano, M.M.: Digital Design, 3rd edn. Prentice Hall, New Jersey (2001)
- Dutta, N.K., Wang, Q.: Semiconductor Optical Amplifiers, 2nd edn. World Scientific Publishing Company, Singapore (2013)
- Hu, H., Zhang, X., Zhao, S.: High speed all-optical logic gate using QD-SOA and its application. *Cogent Phys.* **4**, 13881561/25 (2018)
- Zhang, X., Dutta, N.K.: Effects of two-photon absorption on all-optical logic operation based on quantum-dot semiconductor optical amplifiers. *J. Mod. Opt.* **65**, 166–173 (2018)
- Li, W., Hu, H., Zhang, X., Dutta, N.K.: High speed all optical logic gates using binary phase shift keyed signal based on QD-SOA. *Int. J. High Speed Electron. Syst.* **24**, 1550005 (2015)
- Zhang, X., Li, W., Hu, H., Dutta, N.K.: High speed all-optical encryption and decryption based on two-photon absorption in semiconductor optical amplifiers. *Opt. Commun. Netw.* **7**, 276–285 (2015)
- Dong, H., Wang, Q., Zhu, G., Jaques, J., Piccirilli, A.B., Dutta, N.K.: Demonstration of all-optical logic OR gate using semiconductor optical amplifier-delayed interferometer. *Opt. Commun.* **242**, 479–485 (2004)
- Wang, Q., Dong, H., Sun, H., Dutta, N.K.: All-optical logic OR gate using SOA delayed interferometer. *Opt. Commun.* **260**, 81–86 (2006)
- Kotb, A., Ma, S., Chen, Z., Dutta, N.K., Said, G.: Effect of amplified spontaneous emission on semiconductor optical amplifier based all-optical logic. *Opt. Commun.* **284**, 5798–5803 (2011)
- Kotb, A.: Ultrafast all-optical logic OR gate based on two-photon absorption with a semiconductor optical amplifier-assisted delayed interferometer. *J. Korean Phys. Soc.* **68**, 201–205 (2016)
- Singh, P., Tripathi, D.K., Jaiswal, S., Dixit, H.K.: Design and analysis of all-optical AND, XOR and OR gates based on SOA-MZI configuration. *Opt. Laser Technol.* **66**, 35–44 (2015)
- Singh, P., Tripathi, D.K., Jaiswal, S., Dixit, H.K.: Design of all-optical buffer and OR gate using SOA-MZI. *Opt. Quantum Electron.* **46**, 1435–1444 (2014)
- Kim, J.Y., Kang, J.M., Kim, T.Y., Han, S.K.: All-optical multiple logic gates with XOR, NOR, OR and NAND function using parallel SOA-MZI structures: theory and experiment. *J. Lightwave Technol.* **24**, 3392–3399 (2006)
- Kim, J.Y., Kang, J.M., Kim, T.Y., Han, S.K.: 10 Gbits all-optical composite logic gates with XOR, NOR, OR, and NAND functions using SOA-MZI structures. *Electron. Lett.* **42**, 303–307 (2006)
- Sun, H., Wang, Q., Dong, H., Chen, Z., Dutta, N.K., Jaques, J., Piccirilli, A.B.: All-optical logic XOR gate at 80 Gb/s using SOA-MZI-DI. *IEEE J. Quantum Electron.* **42**, 747–751 (2006)
- Dong, H., Sun, H., Wang, Q., Dutta, N.K., Jaques, J.: All-optical logic operation at 80 Gb/s using semiconductor optical amplifier based on the Mach-Zehnder interferometer. *Microw. Opt. Technol. Lett.* **48**, 1672–1675 (2006)
- Chen, H., Zhu, G., Wang, Q., Jaques, J., Leuthold, J., Piccirilli, A.B., Dutta, N.K.: All-optical logic XOR using a differential scheme and Mach–Zehnder interferometer. *Electron. Lett.* **38**, 1271–1276 (2002)
- Wang, Q., Zhu, G., Chen, H., Jaques, J., Leuthold, J., Piccirilli, A.B., Dutta, N.K.: Study of all-optical XOR using Mach–Zehnder Interferometer and differential scheme. *IEEE J. Quantum Electron.* **40**, 703–709 (2004)
- Kotb, A., Maeda, J.: NXOR based on semiconductor optical amplifiers with the effect of amplified spontaneous emission. *Optoelectron. Lett.* **8**, 437–440 (2012)
- Kotb, A.: Simulation of all-optical logic NOR gate based on two-photon absorption with semiconductor optical amplifier-assisted Mach-Zehnder interferometer with the effect of amplified spontaneous emission. *J. Korean Phys. Soc.* **66**, 1593–1598 (2015)
- Kotb, A.: All-Optical Logic Gates Using Semiconductor Optical Amplifier. Lambert Academic Publishing, Saarbrücken (2012)
- Kotb, A.: Theoretical analysis of soliton NOR gate with semiconductor optical amplifier-assisted Mach–Zehnder interferometer. *Opt. Quantum Electron.* **49**, 1–12 (2017)
- Kotb, A., Zoiros, K.E.: Performance analysis of all-optical XOR gate with photonic crystal semiconductor optical amplifier-assisted Mach–Zehnder interferometer at 160 Gb/s. *Opt. Commun.* **402**, 511–517 (2017)
- Kotb, A.: Computational analysis of solitons all-optical logic NAND and XNOR gates using semiconductor optical amplifiers. *Opt. Quantum Electron.* **49**, 1–17 (2017)
- Kang, I., Rasras, M., Buhl, L., Dinu, M., Cabot, S., Cappuzzo, M., Gomez, L.T., Chen, Y.F., Patel, S.S., Dutta, N.K., Piccirilli, A., Jaques, J., Giles, C.R.: All-optical XOR and XNOR operations at 86.4 Gb/s using a pair of semiconductor optical amplifier Mach–Zehnder interferometers. *Opt. Express* **17**, 19062–19066 (2009)
- Mahad, F.D., Sahmah, A., Supa'at, M., Idrus, S.M., Forsyth, D.: Modeling of semiconductor optical amplifier gain characteristics for amplification and switching. In: Proceedings of AIP Conference, vol. **1341**, pp. 217–220 (2011)
- Kumar, Y., Shenoy, M.R.: Enhancement in the gain recovery of a semiconductor optical amplifier by device temperature control. *Pramana J. Phys.* **87**, 82 (2016)
- Schares, L., Schubert, C., Schmidt, C., Weber, H.G., Occhi, L., Guekos, L.: Phase dynamics of semiconductor optical amplifiers at 10 to 40 GHz. *IEEE J. Quantum Electron.* **39**, 1394–1408 (2003)
- Melo, A.M., Petermann, K.: On the amplified spontaneous emission noise modeling of semiconductor optical amplifiers. *Opt. Commun.* **281**, 4598–4605 (2008)
- Siarkos, T., Zoiros, K.E., Nastou, D.: On the feasibility of full pattern-operated all-optical XOR gate with single semiconductor optical amplifier-based ultrafast nonlinear interferometer. *Opt. Commun.* **282**, 2729–2734 (2009)